Martensitic transformations in nonferrous shape memory alloys

K. Otsuka *, X. Ren

Institute of Materials Science, University of Tsukuba, Tsukuba, Ibaraki 305-8573, Japan

Abstract

In the present paper, the important developments on martensitic transformations in non-ferrous shape memory alloys within nearly 10 years are critically reviewed. Since the alloys include not only noble-metal alloys but also Ti–Ni based alloys, the field is very wide both in contents and in the kind of alloys. We tried to describe items with uniformity, which are common to all alloys, but specific items were also discussed when they are important. Special attention was paid to similarity and dissimilarity among alloys to highlight key points on the issues concerned. The topics include the following: (1) phase diagrams, (2) crystal structures of martensites, (3) crystallography of martensitic transformations, (4) R-phase transformation, (5) pre-transformation phenomena and origin of martensitic transformation, (6) martensite aging and rubber-like behavior, (7) martensite and deformation. © 1999 Elsevier Science S.A. All rights reserved.

Keywords: Martensitic transformation; Shape memory alloys; Nonferrous; Ti–Ni; pre-transformation

1. Introduction

The subjects, that the present authors were given, include not only noble metal-based alloys but also Ti–Ni based alloys. Thus, these include nearly all shape memory alloys (SMA), except for ferrous ones, and it is difficult to discuss them all within limited pages. For this reason, we confine ourselves to the studies, in which substantial progress has been made in *nearly* the last 10 years. Because of the diversity of the subjects covered, we pick up rather general problems mostly, but we also pick up some specific ones, in case the specific one is related to an important general problem. In reviewing the above issues, we specifically pay attention to similarity and dissimilarity among alloys, by which the characteristics of each behavior will be clarified.

2. Phase diagrams

The phase diagram is a basis to understand all kinds of phase transformations including martensitic ones. It is also vitally important to control the microstructure

of an alloy, by which physical properties of the alloy are improved. In the present section, we introduce two phase diagrams of Ti–Ni and Ni–Al alloy systems, both of which were controversial for many years, and were finally determined fairly recently. The former is important, because the phase diagram is actively utilized to improve the shape memory (SM) characteristics of the important shape memory alloys (SMA), while the latter is important, because the Ni_5Al_3 phase appearing in the alloy system suppresses the reverse transformation of the Ni–Al alloy, leading to the annihilation of the shape memory effect (SME) in the alloy, as will be explained in detail later.
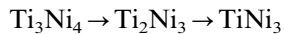
Fig. 1 is a recent phase diagram by Massalski et al. [1], which is slightly modified by the present authors, as will be explained later. In the phase diagram our interests are restricted in the central region bounded by Ti_2Ni and $TiNi_3$ phase, including the TiNi phase, which transforms martensitically from B2 to B19′. The first dispute on the phase diagram started between Duez and Taylor [2], and Margolin et al. [3]. Duez and Taylor reported the eutectoid decomposition of TiNi into Ti_2Ni and $TiNi_3$ at around 650°C, and Margolin et al. denied the decomposition and asserted a wide solubility limit of TiNi down to ambient temperature. Then, Poole and Hume-Rothery [4] made a thorough examination of the phase diagram. They found that the solubility limit on Ti-rich side is nearly vertical, while

---

* Corresponding author. Tel.: + 81-298-53-5294; fax: + 81-298-55-7440.

E-mail address: otsuka@mat.ims.tsukuba.ac.jp (K. Otsuka)

that on Ni-rich side decreases quickly with decreasing temperature, supporting the eutectoid decomposition at 650°C by Duez and Taylor. In 1971, Wasilenski et al. [5] found a new phase Ti_2Ni_3 between TiNi and $TiNi_3$, and proposed a peritectoid reaction at 625°C. However, this peritectoid reaction has never been confirmed. Meanwhile, Koskimaki et al.[6] found the 'X-phase', which is now known as Ti_3Ni_4 phase, and they claimed that the X-phase is an intermediate phase prior to the eutectoid decomposition into Ti_2Ni and $TiNi_3$. Thus, the understanding of the phase diagram was chaotic by that time.

A unified understanding came thereafter by an extensive study by Nishida et al.[7], who utilized metallography, electron microscopy and EDS (Energy Dispersive X-ray Spectroscopy). By making detailed TTT diagrams, they showed that the $TiNi_3$ phase is an equilibrium phase, while both Ti_3Ni_4 and Ti_2Ni_3 phases are intermediate ones toward $TiNi_3$, which appear in the following order with aging time:

$$Ti_3Ni_4 \rightarrow Ti_2Ni_3 \rightarrow TiNi_3$$

Thus, the eutectoid decomposition was denied, and the phase diagram in the present system was established. In Fig. 1, the dotted line at 630°C indicating the eutectoid decomposition, which is present in the original phase diagram by Massalski et al. is deleted, following the above work. The order-disorder transition temperature at 1090°C [8] is also added by a dotted line in the figure. The composition of the X-phase, and the struc-
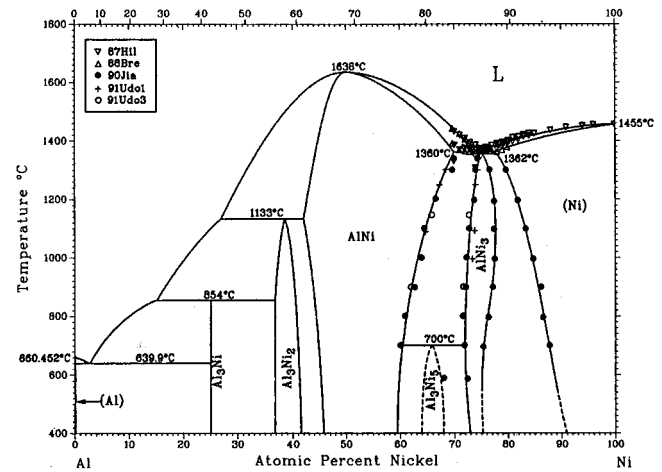
Fig. 2. Phase diagram of Ni–Al alloy by Okamoto [17].

ture of the Ti_3Ni_4 phase were controversial for many years, but they had been solved [9–11]. The structure belongs to space group $R\bar{3}$ with a rhombohedral unit cell. See original papers for details [10,11].

This phase diagram is now extensively used to improve SM characteristics of this most important SMA. For example, on the Ni-rich side the finely dispersed Ti_3Ni_4 precipitates are known to be very effective to improve SM and superelastic (SE) characteristics [12,13]. They are also used to realize the R-phase transformation, which is very useful for actuator applications of SMA with a very small temperature hysteresis (1–2 K) [14]. The presence of the aligned precipitates is also responsible for the realization of the all round shape memory effect [15]. On the other hand, precipitation hardening by the Ti_2Ni phase can not be used on the Ti-rich side in bulk materials, because the solubility limit is almost vertical on the Ti-rich side. However, in sputter-deposited films, in which the B2 parent phase is produced through an amorphous state followed by crystallization, precipitation hardening of Ti_2Ni phase can be utilized, since any amount of Ti can be soluble in the amorphous state. This will be discussed in detail in this conference [16].

We now discuss the phase diagram of the Ni–Al alloy system. Fig. 2 is a most recent phase diagram by Okamoto [17]. Again we are interested only in the central region of NiAl, which transforms martensitically from B2 → 3R (2M) or 7R (14M). Our crucial concern is on the Ni_5Al_3 phase. This phase was first found by Enami and Nenno in 1978 [18], as a product, when a 3R (2M) martensite was heated. Since this phase was observed invariably through 3R (2M) martensite after a certain period [18–20], whether the phase is an equilibrium one or not was controversial [21,22]. However, it was later confirmed that 3R martensite plus B2 NiAl microstructure in the asquenched state transformed nearly completely to the
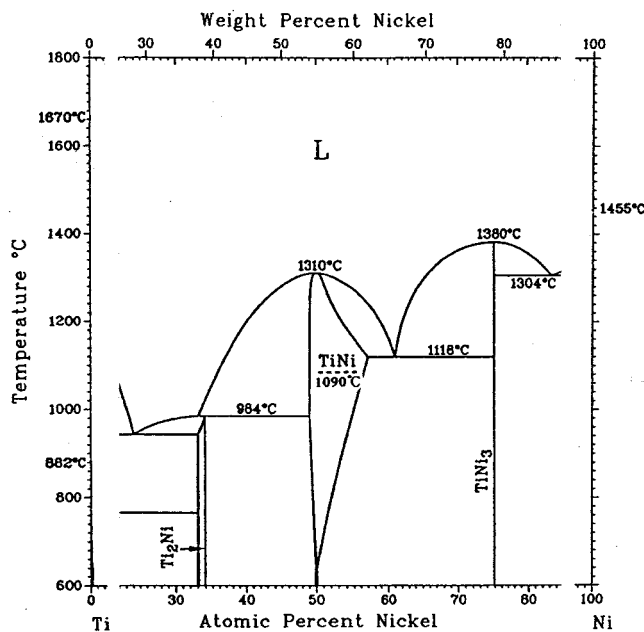

Fig. 1. Phase diagram of Ti–Ni alloy by Massalski et al. [1] The original phase diagram is slightly modified such that a dotted line at 630°C for eutectoid decomposition is deleted and a dotted line is added at 1090°C for order–disorder transition for Ti–Ni. See text for more details.

Ni_5Al_3 phase upon aging at 823 K for 720 h [23]. Thus, it is now confirmed to be an equilibrium phase. The structure of the Ni_5Al_3 phase is of the Pt_5Ga_3-type with an orthorhombic unit cell [18,19].

The transformation from the martensite to the Ni_5Al_3 phase is a diffusion-controlled transformation [18–23]. Thus, when the A_f temperature (reverse transformation finish temperature) is low, the presence of the Ni_5Al_3 phase is not a problem for the reverse transformation nor for the SME. In the case of the Ni–Al alloy system, the structure of the martensite changes from 3R (2M) to 7R (14M) around the composition of Ni–37at%Al. For Al ≥ 37%, the structure of martensite is 7R (14M), and A_f becomes depressed below room temperature, while for Al ≤ 37%, the structure of martensite is 3R (2M), and A_f increases with decreasing Al content [24]. Thus, for low Al content Al < 36%, the reverse transformation is suppressed greatly, and we can not expect a good SME, because the reordering (decomposition) from the martensite to the Ni_5Al_3 phase occurs so easily [21,22]. The problem discussed above is very similar to the decomposition problem in Cu-based SMA. However, it will be more severe than the latter, since the reordering of the martensite to Ni_5Al_3 occurs so easily at high temperature.

3. Crystal structures of martensites

To know the crystal structure of a martensite is a first step toward understanding the mechanism of the martensitic transformation. Strictly speaking, however, what is required in the phenomenological theoretical calculation are lattice parameters and the lattice correspondence between parent and martensite, and exact atom positions are not required, since small shuffles are considered not to contribute to the shape strain. However, in the electron band structure calculation of martensite, which is a new trend in the research of martensitic transformations, an accurate structure of martensite is indispensable. In fact a correct band structure of martensite can not be obtained unless accurate atomic parameters are used. Since martensites usually appear in a self-accommodating manner, a single crystal of martensite is not usually obtained. However, by utilizing the stress-induced martensitic transformation technique, it is now possible to make such single crystals. Thus, in this section we first introduce the structures of martensites accurately determined by a X-ray four-circle diffractometer and the least squares analysis.

In Au–Cd alloys two types of martensites appear depending upon Cd content: γ_2' (B19) martensite appears near Au–47.5% Cd, while ζ_2' martensite appears near Au–50.0% Cd. The structure of the γ_2' martensite with an orthorhombic unit cell was determined by Ölander [25], and was later refined by Ohba et al. [26]

See the original paper for detailed atomic parameters. The structure of the ζ_2' martensite was unsolved for over 50 years, but finally it was solved by the same authors by the same technique [27]. Surprisingly, the space group is P3, which has no center of symmetry. They further showed by numerical simulation that the structure can be made by the superposition of the following three transverse displacement waves and their higher harmonics.

$$\tfrac{1}{3}\langle 011\rangle\langle 0\bar{1}1\rangle + \tfrac{1}{3}\langle \bar{1}01\rangle\langle 101\rangle + \tfrac{1}{3}\langle 110\rangle\langle 1\bar{1}0\rangle$$

From this mechanism, phonon softening is expected at the 1/3 position of the $\langle 110\rangle$ TA_2 branch of the phonon–dispersion curve. This phonon softening was actually observed later by neutron inelastic scattering measurements [28].

We now discuss the structures of martensites in Ti–Ni or Ti–Ni–X (X = Cu or Fe etc.) alloy systems. Three types of structures appear depending upon composition. Among these, the most common one is a monoclinic (B19′) martensite, which is observed in Ti–Ni binary alloys and in most of the ternary alloys. The second one is the so-called R-phase, which appears in Ti–Ni–Fe and in aged or thermomechanically treated Ni-rich binary Ti–Ni alloys. Since the R-phase transformation occurs prior to the onset of the monoclinic martensite transformation, the former was often called a pre-martensitic transformation, but it is well established that the R-phase transformation is a martensitic transformation, which competes with the monoclinic martensitic transformation. The third one is an orthorhombic martensite (B19), which appears in Ti–(50 − x)Ni–xCu (x ≧ 7.5) alloy. Since the accurate structures of the monoclinic martensite and the R-phase were determined, we discuss the first two in the following.

It took a long time until the structure of the monoclinic martensite was determined accurately by Kudoh et al. [29] after the first discovery of the phase by Purdy and Parr [30]. See Ref. [29] for historical developments [31–34]. The space group is $P2_1/m$ with a monoclinic unit cell. The accurate atomic parameters and lattice parameters are given in the original paper. This structure is quite unique, because the structure is not observed in any alloy other than Ti–Ni based alloys, although most of the β-phase alloys with a B2 ordered structure in parent usually transform into long period stacking order structures. This uniqueness is related with temperature dependence of elastic constants in these alloys, as will be discussed in Section 6.2.

The structure of the R-phase in Ti–Ni based alloys have also been controversial for many years after the first finding of the phase by Dautovich and Purdy in 1965 [35]. The R-phase is also related with a delicate problem of a pre-transformation behavior, but this will be discussed in Section 5, and only the structure will be

discussed in this section. Vatanayon and Hehemann [36] were the first who noted the similarity of the structure of the R-phase and that of the ζ_2' phase in Au–Cd discussed above, since both electron diffraction patterns were similar. Thus, they suggested P$\bar{3}$1m as a possible space group. Then, Goo and Sinclair [37] studied the structure by CBED (convergent beam electron diffraction) technique, and reported that the space group is P$\bar{3}$1m, but they did not determine the atomic parameters. Very recently Hara et al. [38] finally determined the structure. The space group they reported is P3 instead of P$\bar{3}$1m, and the atomic parameters were determined with *R*-factor (reliability factor) $R_{wp} =$ 8.19%. We will introduce their analysis briefly in the following. Since the structure of the ζ_2' phase in Au–Cd was determined to be P3 as discussed above, P3 is also another possible candidate for the space group of the R-phase. Thus, they took both P$\bar{3}$1m and P3 into considerations as possible space group candidate, and carried out very careful analysis by combining various techniques such as electron diffraction (with static and dynamic analysis), CBED and X-ray powder diffraction with Pawly analysis and Rietveld analysis. Although the difference between P3 and P$\bar{3}$1m was much smaller for the R-phase compared with that for the ζ_2' Au–Cd martensite, the results of the careful analysis all favored space group P3, and the atomic parameters were determined by the Rietveld analysis. The distinction between P3 and P$\bar{3}$1m lies in that although the atomic coordinates *x* and *y* of the (3d) site are close to the mirror plane of P$\bar{3}$1m, the atomic coordinates *z* are not close to the mirror plane of P$\bar{3}$1m. In the case of ζ_2' Au–Cd martensite this deviation in *z* is large, while in the R-phase it is small, and this difference made it difficult to distinguish P3 and P$\bar{3}$1m. The structure of the R-phase finally obtained is shown in Fig. 3. See the original paper for the details of the atomic parameters and lattice parameters etc. Since the true structure is not rhombohedral but trigonal, the term R-phase is not adequate, and the term T-phase is more appropriate. However, to change the terminology may be confusing.

4. Crystallography of martensitic transformations

The crystallography of martensitic transformations (MT) was extensively reviewed in ICOMAT-89 from phenomenological theoretical point of view [39]. It was shown that the theory and experiment agree well in most cases, if we choose the lattice invariant shear (Type I twinning or Type II twinning) correctly. We will introduce the development thereafter briefly in this section. The remaining two problems were the B2–ζ_2' transformation in Au–Cd and the {225} transformation in ferrous alloys. Among these the former one was solved, leaving the latter. The essential problem in the

B2–ζ_2' transformation was whether the lattice invariant shear is present or not in this transformation, since Tadaki et al. [40] reported that there is no lattice invariant shear, while other researchers like Ledbetter and Wayman [41] assumed or reported {011} twinning. However, according to our recent works [42,43], both were correct, as will be explained later, i.e. two types of transformations with or without lattice invariant shear are possible in the alloy system, since the transformation strains are so small in the present alloy system. First we will introduce the result of comparison between theory and experiment in Fig. 4, which was carried out for stress-induced MT above M_s (martensite start) temperature. In this case, the lattice invariant shear was invariably present, but it was {001} twinning instead of {011} twinning as Ledbetter et al. reported previously. In Fig. 4 the habit plane (p$_1$) and twin plane (K$_1$) are plotted in a reduced form in a unit stereographic triangle, but they and their orientation relationships were consistent with theory in all respects. Thus, we can conclude that theory and experiment agreed well in the present transformation. The difference between the calculated habit plane by us and that by Ledbetter and Wayman is due to the difference in the used lattice parameters. Since the transformation strain in the present transformation is so small, the accuracy in lattice parameters greatly affects the calculated habit plane. In our case the lattice parameters of parent and martensite were accurately measured at 306 and 303 K,
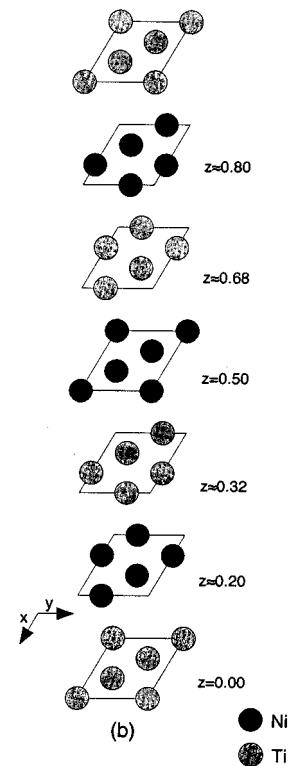

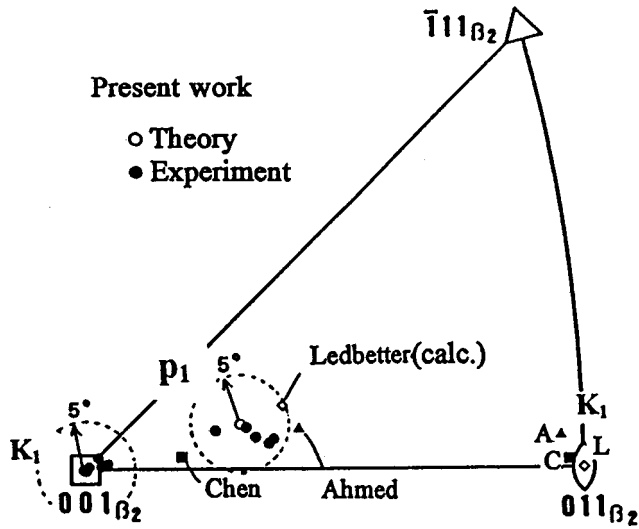Fig. 3. Structure of the R-phase (space group P3) [38].

Fig. 4. Comparison between theory and experiment for B2–ζ_2' transformation in Au–49.5Cd alloy [43]. $\mathbf{p}_1$ and $\mathbf{K}_1$ represent habit plane and twin plane respectively. A, C, L represent $\mathbf{K}_1$ plane reported by Ahmed, Chen and Ledbetter, respectively.

respectively, the difference in temperature being only 3 K apart. The K_1 planes were invariably {001}, although {011} planes are also possible twinning planes from a theoretical point of view, since both are mirror planes in the parent phase.

We now discuss the self-accommodation of the above martensite. From an optical micrograph of Fig. 5(a), we can observe two types of morphologies (A) and (B). We call the former 'roof' type and the latter 'herring-bone' type. The essential difference between the two lies in that {001} twinning as a lattice invariant shear are present in the 'roof' type, while lattice invariant shear is absent in the 'herring-bone' type. These self-accommodations were analyzed quantitatively as shown in Fig. 5(b, c), using the shape strain matrix and the deformation matrix respectively. The 'roof' type morphology consists of four habit plane variants as shown, while the 'herring-bone' type morphology consists of four correspondence variants as shown. As a result of the calculations, both types of self-accommodations were shown to release strains due to the formation of one variant efficiently. In another words, in the present transformation the transformation strains are so small, that two types of transformations with and without lattice invariant shear are possible. Thus, the discrepancy between Ledbetter and Wayman, and Tadaki et al. were rationalized. As discussed in Section 3, the structure of the ζ_2' martensite and the R-phase in Ti–Ni based alloys are essentially the same. Thus, the self-accommodation is expected to be the same in the two alloys. In fact, the self-accommodation in Fig. 5(c) is the same as that of the R-phase previously reported by Fukuda et al. [44] However, the 'roof-type' morphology has not been found in the R-phase, although the reason is not known as yet.
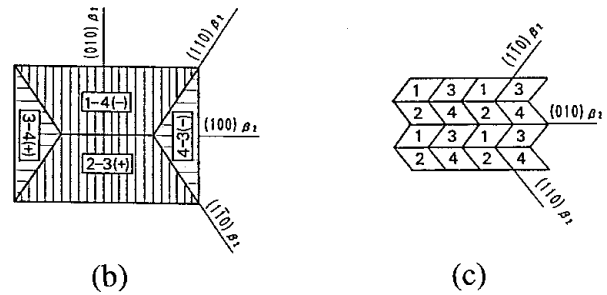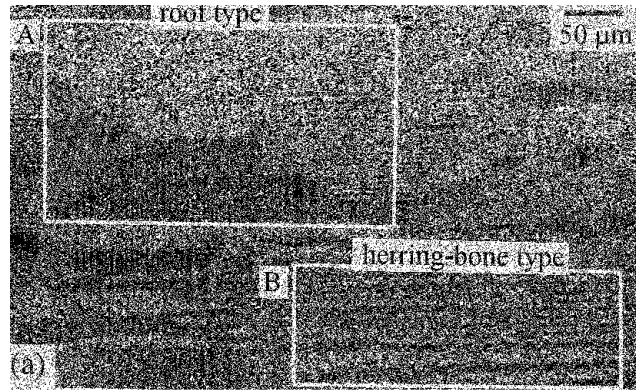

Fig. 5. (a) A typical optical micrograph of two distinct morphologies of the ζ_2' martensite in Au–49.5Cd alloy: (A) 'roof' type and (B) 'herring-bone' type [42]. (b) and (c) Results of the crystallographic analysis of the two self-accommodating morphologies for (b) 'roof' type and (c) 'herring-bone' type. The numbers such as 3–4 (+) etc. in (b) represent habit plane variants, while those in (c) correspondence variants [42].

Saburi et al. [45] made a systematic work on the self-accommodation of martensites in β-phase alloys, which transforms from ordered BCC to long period stacking order structures. They showed that four habit plane variants around $\langle 011 \rangle_{B2 \text{ or } DO3}$ pole make a self-accommodating group such that the strains created by each variant upon transformation cancel each other.
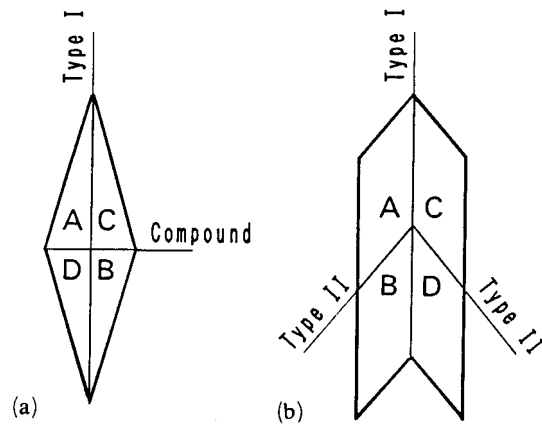

Fig. 6. Scheme of the basic morphology of self-accommodation for (a) the diamond morphology and (b) the parallelogram morphology [24]. See text for details.
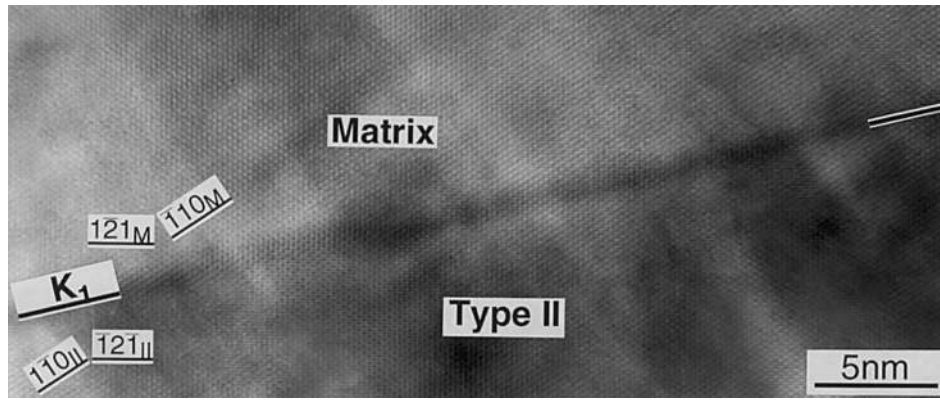
Fig. 7. HRTEM micrograph of Type II twin boundary in Cu–Al–Ni martensite, beam // η_1 twinning shear direction [48]. See text for details.

Thus, they proposed Fig. 6(a) as a basic morphology of self-accommodation. Murakami et al. [24] carried out a similar analysis for the B2–7R (14M) transformation in a Ni–Al alloy thereafter, and obtained the similar result with respect to the combination of the four variants. However, they found that the basic morphology of self-accommodation is not like Fig. 6(a) but like Fig. 6(b), because the introduction of compound twin does not accommodate strains, while both Type I twin and Type II twin accommodate strains effectively. The basic morphology of Fig. 6(b) applies not only for 7R (14M) martensite but also for other martensites such as 3R (2M) and 9R (6M) etc.

As discussed earlier, Type II twinning becomes a lattice invariant shear in some alloys such as Ti–Ni, Cu–Al–Ni, Cu–Sn etc. Since Type II twins have irrational twin boundary, the physical meaning of the irrational boundary is a big problem. Christian-Crocker [46] and Knowles [47] proposed that an irrational boundary consists of rational ledges and steps, the average being irrational. Furthermore, Knowles presented a HRTEM (high resolution transmission electron microscopy) micrograph of the irrational boundary in Ti–Ni alloy, as if consisting of rational ledges and steps. However, the micrograph was taken in non-edge-on condition, since the edge-on condition for an irrational boundary is unique in Type II twinning, i.e. η_1 (twinning shear direction) direction. Thereafter, Hara et al. [48,49] carried out a careful study to observe $\langle 111 \rangle$ Type II twin boundary in a Cu–Al–Ni alloy by HRTEM, but they could not observe ledges nor steps even in the unique η_1 direction. One typical example in edge-on condition is shown in Fig. 7. The characteristics of the boundary is that the boundary is always associated with dark strain contrast, and the lattice is continuous through the irrational boundary. Nishida et al. [50] also made extensive studies on the $\langle 011 \rangle$ Type II twin boundary in Ti–Ni by HRTEM, but they did not observe ledges nor steps either. Based on these experimental results, it is most likely that Type

II twin boundary are irrational even on a microscopic scale, and the strains at the boundary is elastically relaxed with wide twin widths, thus leaving a strain contrast as in Fig. 7. To confirm this interpretation, Hara et al. [49] carried out computer simulation by molecular dynamics method, with the initial condition of twin boundary, which consists of ledges and steps, and are in Type II twin orientation to each other. Then, the result of simulation was found to have ended up with irrational twin boundary without ledges or steps. Thus, the above interpretation for an irrational twin boundary was justified.

5. R-phase transformation

The R-phase transformation in Ti–Ni–Fe alloys or in thermally treated Ti–Ni alloys attracted much attention until recently, because of the curious transformation behavior and actuator applications due to a very small temperature hysteresis. Thus, many researches have been done (See Ref. [51,52] for historical developments.), but most extensive and intensive among these are those by Salamon-Wayman's group [51,53–56], who utilized various techniques such as neutron and X-ray diffraction, neutron inelastic scattering, TEM, electrical resistivity, magnetic susceptivility and specific heat etc. As a result, they found by neutron diffraction that the superlattice reflections appear at an incommensurate position first, and the incommensurability decreases with decreasing temperature until it locks-in to a commensurate phase (i.e. R-phase) at a lower temperature [53,55]. Accompanying with this is a change in the α angle (rhombohedral angle) with lowering temperature, which starts from 90° in the parent phase [53,57]. They claim that the change in the α angle coincides with the above lock-in temperature [53]. They also found a phonon softening at $1/3 \langle 110 \rangle \langle 1\bar{1}0 \rangle$ TA$_2$ branch [56]. Based on these results, they ascribed the transformation due to the formation of charge density

waves (CDW) [51,55]. On the other hand, Shapiro et al. [54] made a detailed study on the incommensurate state by the X-ray diffraction technique using a linear position sensitive detector, and reported that the incommensurate displacement in reciprocal space is not regular nor periodic. Thus, they denied the interpretation by CDW. This peculiar incommensurability is not understood well, although there is a 1-dimensional model called the 'Modulated Lattice Relaxation' model by Yamada [58].

Thus, the present status of understanding the R-phase transformation may be summarized as follows [51,53]. It occurs in two stages from B2 to incommensurate(I) to commensurate(C). The temperature T_r where the incommensurate superlattice reflections start to appear coincides with that where the restivity (ρ) starts to rize or the magnetic susceptibility (χ) starts to change. The lock-in temperature, T_I, from incommensurate to commensurate coincides with the temperature where $d\rho/dT$ or $d\chi/dT$ becomes maximum. The lattice distortion is absent (i.e. $\alpha = 90°$) between T_I and T_r, even though superlattice reflections are present. The temperature difference between T_I and T_r in the case of Ti–46.8Ni–3.2Fe single crystal is 8 K. The transformation from B2 to I is considered to be 2nd order and to be hysteresis free. At T_r, R-phase domains appear as a result of the introduction of the lattice distortion due to lock-in. With decreasing temperature below T_r, the lattice distortions increase, because the α angle decreases further away from 90°.

Meanwhile, Saburi et al. [44,59] made a qualitative study on the R-phase transformation by electron microscopy observations of a Ti–48Ni–2Al alloy by beam heating. They observed that the R-phase nucleates from lattice defects such as dislocations and grow in a cooling process. Thus, they claimed that the transformation is first order. They also reported that the specimen is in a diffuse incommensurate state above the temperature, where the resistivity starts to increase.

More recently Tamiya et al. [52] carried out a detailed study by in situ electron microscopy observations with a cooling stage and imaging plates (IP). First they measured the resistance vs. temperature curve very accurately. Although the temperature hysteresis was as small as 0.7 K, the temperature hysteresis was present from the starting temperature of resistance increase (R_s) upon cooling. This means that the transformation is 1st order throughout the process. They also observed that parent (P) and R-phase (R) coexist in the temperature range between R_s and R_f (finish temperature of rapid resistance increase), as shown in Fig. 8. This is a clear manifestation that the transformation is first order, being consistent with Saburi's report. Then they measured accurately the distance between superlattice spots by using 'image gauge' etc. on a computer, and they concluded that within experimental errors the R-phase
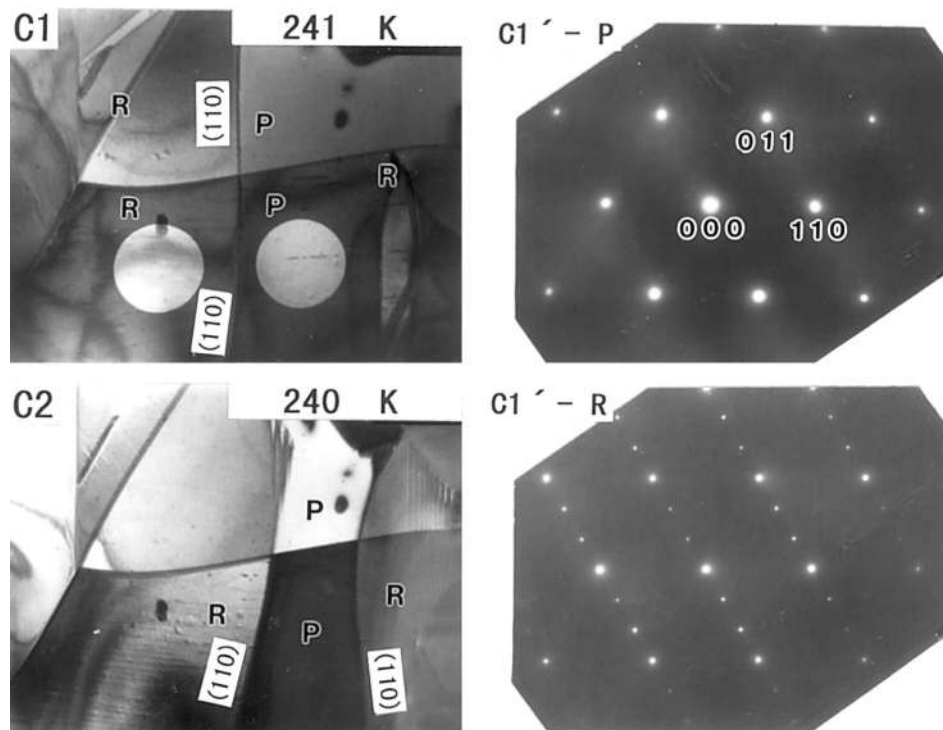

Fig. 8. In situ observations of the R-phase transformation upon cooling. Electron diffraction patterns were taken from the encircled regions in the corresponding micrograph. The letters 'P' and 'R' represent parent phase and R-phase respectively, as confirmed by the corresponding diffraction patterns [52].

is in commensurate state from the beginning. This means that there is no incommensurate state at temperatures below R_s. In Fig. 8(C1′–P) we can hardly see superlattice reflections. However, by using a new 'energy filter' technique, a diffuse and incommensurate superlattice reflections were observed. These diffuse superlattice reflections were observed at temperatures above R_s as well. The diffuseness assessed by FWHM (full width at half maxim) was one order of magnitude higher than that of the commensurate R-phase. These observations deny the above view by Salamon and Wayman, which has been accepted until recently.

From these recent studies it seems now clear that the R-phase transformation is 1st order throughout, and the region between R_s and R_f characterized by a temperature hysteresis simply represents a two-phase region consisting of parent and R-phase. Furthermore, diffuse incommensurate superlattice reflections are present in the parent phase at temperatures well above R_s [60,61], although we still do not know what these diffuse superlattice reflections represent. We will show in the following that the present view is very similar to that of the B2–ζ_2' transformation in Au–Cd.

The B2–ζ_2' martensitic transformation in Au–Cd is also associated with a sharp increase of resistivity upon cooling with a small temperature hysteresis 1–2 K. It is quite clear that the narrow temperature region with the hysteresis represents a two-phase region of parent and martensite [40,42]. Besides, Noda et al. [62] reported that at temperatures above Ms diffuse superlattice reflections are present at around $1/3\langle 110 \rangle^*$ position in reciprocal space, which are incommensurate and non-periodic. Thus, the transformation behavior in this alloy is very similar to the R-phase transformation. However, there is another report stating that the diffuse superlattice reflections are commensurate and time-dependent [63]. Thus, more careful and detailed studies are required for these very peculiar transformations in the above two alloys.

6. Pre-transformation phenomena and the origin of the martensitic transformation

The pre-transformation phenomenon is an important issue in martensitic transformation, because it is closely related to the origin of MT and to a better understanding of martensite structure. However, it is also the most challenging and most controversial issue in MT. Below we start with a general description of pre-transformation phenomena in the whole spectrum of MT from 2nd order, weakly 1st order to strongly 1st order, and highlight the problems unsolved, then introduce some recent progress in understanding pre-transformation phenomena in shape memory Ti–Ni and β-phase alloys. Finally, we briefly discuss the origin of MT from a viewpoint of lattice dynamics.

6.1. Pre-martensitic phenomena in the whole spectrum of martensitic transformations, from 2nd order, weakly 1st order, moderately 1st order, to strongly 1st order

MT can be either of second order or of first order although the latter is dominant. In fact, there is a continuous spectrum of MTs from 2nd order, weakly 1st order, moderately 1st order, to strongly 1st order, which depends on the magnitude of transformation strain or volume change to be zero, near-zero, moderate, or large. We can see there seems to exist an interesting correlation between this continuous spectrum of transformations and corresponding precursor phenomena.

2nd order transformations (e.g. A15 compounds and some inorganic compounds) exhibit complete lattice softening ($c' = 0$ or zero phonon energy) at the transformation temperature [64,65]. Weakly 1st order transformation (e.g. In–Tl) behaves very similar to 2nd order transformation in many aspects, including a near-zero elastic or phonon softening [66]. Shape memory alloys undergo moderately 1st order transformations. They exhibit incomplete lattice softening and moderate temperature dependence [67]. Strongly 1st order transformations seem to exhibit weaker lattice softening with weaker or little temperature dependence. Ferrous alloys and alkali metals belong to this group, and in particular the latter appear to exhibit little anomaly prior to MT (the $TA_2\langle 110 \rangle$ phonon branch, although soft, has little temperature dependence and has no dip [68,69]). Therefore, it seems to exist a continuous spectrum of precursor phenomena: with the gradual change of the MT from 2nd order to strongly 1st order, the extent of precursory lattice softening seems to decrease and becomes less temperature dependent. However, present available theories can explain only part of the spectrum. Soft-mode theory successfully explained 2nd order MTs [70], but is not applicable to 1st order MTs where mode softening is incomplete or non-existent. On the other hand, a theory by Krumhansl and Gooding [71] explained the main features of 1st order MT including incomplete lattice softening by considering the important role of anharmonicity, and suggested that anharmonicity is the driving force of 1st order MT. However, they also pointed out that weakly 1st order MT is still a challenging problem to be solved because it behaves very similar to 2nd order MT. Above all, it is important but rather challenging to understand the whole spectrum of precursor phenomena.

6.2. Pre-transformation softening in Ti–Ni (including Ti–Ni–based alloys) and origin of the B19′ martensite

Martensite structures of most shape memory alloys (ordered bcc) can be viewed as different stacking of {110} planes (here we call basal plane) of the parent
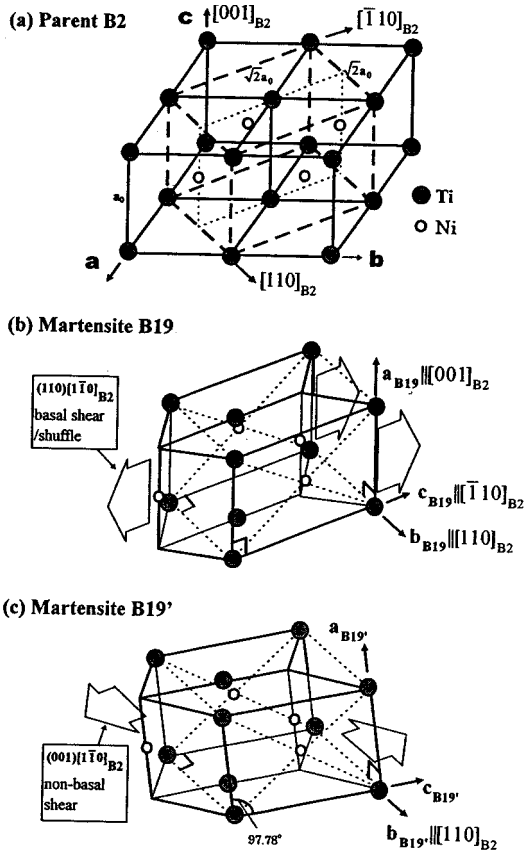
Fig. 9. Structural relationship among cubic parent phase (B2) and two kinds of martensites B19 and B19'. (a) the parent phase B2 cells with a fct cell outlined; (b) orthorhombic martensite B19, formed by shear/shuffle of the basal plane $(110)_{B2}$ along $[1\bar{1}0]$ direction; (c) monoclinic B19' martensite of Ti–Ni, formed by a non-basal shear (001) $[1\bar{1}0]_{B2}$ to the B19 structure [73].

phase by $\{110\}\langle 1\bar{1}0\rangle$ shear/shuffle, such as 2H (B19), 3R, 6R, 7R, 9R and 18R. The formation of such martensites is in agreement with Zener's idea [72] and its modern version (lattice softening) that bcc structure is unstable with respect to $\{110\}\langle 1\bar{1}0\rangle$ shear/shuffle, as manifested by the softening in c' and related TA$_2$ phonon mode. However, the B19' martensite of Ti–Ni-based alloys possesses a unique monoclinic structure, which can be viewed as a conventional basal structure B19 being distorted by a non-basal shear $\{001\}\langle 1\bar{1}0\rangle$ (Fig. 9) [32,73]. It is puzzling why a non-basal shear is produced, and obviously this fact cannot find an answer in the conventional basal shear/shuffle theory.

A key to understanding the origin of the non-basal shear in B19' martensite was proposed recently by Ren and Otsuka [73]. They noticed that the elastic constant associated with this non-basal shear is c_{44} (c_{44} also represents $\{001\}\langle 100\rangle$ shear resistance by definition). If this non-basal shear mode is softened enough and couples with the basal shear/shuffle mode, the resultant martensite will incorporate both basal shear/shuffle and this non-basal shear, leading to the B19' structure. In

fact, it has been known for a long time that elastic softening in Ti–Ni exhibits an anomalously low anisotropy factor $A = c_{44}/c'$ (≈ 2) as a result of low-lying and softening c_{44} [74] as shown in Fig. 10, in sharp contrast to any other martensitic alloys. However, the correlation between this unique behavior and the unique B2–B19' transformation was not exploited. From the above view, it becomes clear that the softening in c_{44} is a necessary step to introduce the non-basal shear $\{001\}\langle 1\bar{1}0\rangle$ into the martensite, and the incorporation of this non-basal shear into MT is realized through its coupling with the basal shear/shuffle strain mode. The coupling between the basal shear and $\{001\}\langle 1\bar{1}0\rangle$ non-basal shear can be seen from the decreasing anisotropy c_{44}/c' towards MT for Ti–Ni, which transforms from B2 into B19', as shown in Fig. 10(b). This behavior has never been found in other shape memory alloys transforming into basal plane martensite structures.

According to the above idea, we can deduce that if the coupling between basal shear and the non-basal shear is weakened by alloying, the non-basal shear will not be incorporated into the transformation and the resultant martensite structure does not contain the non-basal shear. To verify this prediction, we measured elastic constants of Ti–30Ni–20Cu alloy [75,76], and
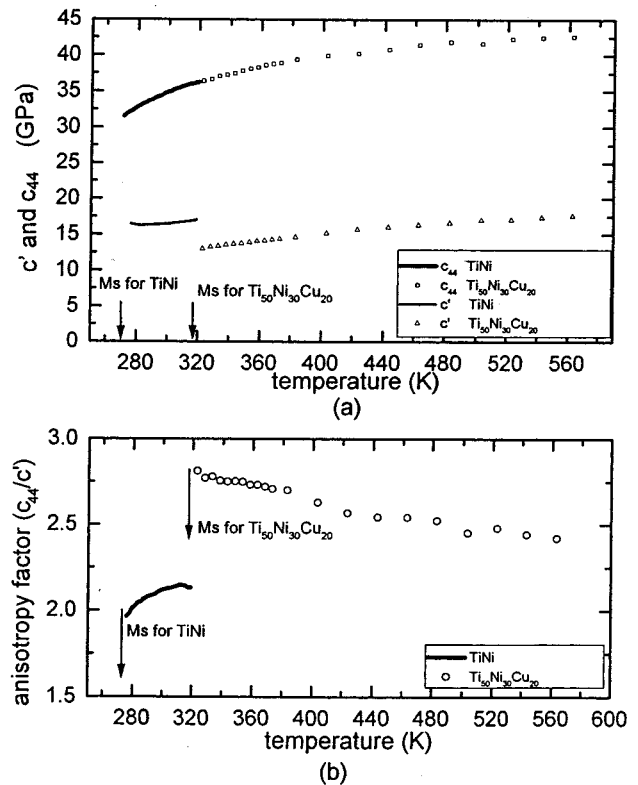

Fig. 10. A comparison of the temperature dependence of elastic constant c' and c_{44} (a), and anisotropy factor $A = c_{44}/c'$ (b) between Ti–Ni alloy [74] and Ti–30Ni–20Cu alloy [75,76] above martensitic transformation temperature [73].

found that its elastic anisotropy exhibits an increase with approaching MT as shown in Fig. 10(b), in contrast to Ti–Ni, although both alloys exhibit softening in c' and c_{44}. This indicates a weakened coupling between basal shear and the non-basal shear. The result of this weakening in coupling is well known: Ti–30Ni–20Cu alloy transforms from B2 into a basal structure B19 without the non-basal monoclinic shear [77]. Thus this result gives a strong support to the above view. An important conclusion we can draw from understanding the B2–B19′ transformation is that MT as a whole can include a non-basal strain mode, as long as such a mode has a strong coupling with the basal strain mode, and conventional basal strain picture of MT is not generally valid.

The Ti–Ni-based alloy has also been known to transform into a different martensite called R phase under certain conditions (which has been frequently mistaken for a precursor of B19′ martensite). Now we know that B2–R is also a 1st order MT, and R–B19′ is a martensite-to-martensite transformation. Section 6.1 gave a detailed discussion on R-phase transformation.

6.3. Pre-transformation phenomena in β-phase alloys

Precursor phenomena in β-phase shape memory alloys have been studied for a long time using various methods [78]. These alloys can be classified as undergoing moderately 1st order MT with transformation strain of one to several percent. Even within this class of MT, we can still see the variation of the precursory lattice softening with transformation strain (which represents the 'strength' of 1st order transformation). For example, the B2–ζ_2' transformation of equiatomic Au–Cd involves very small transformation strain ($\approx 0.8\%$), and recent neutron inelastic scattering measurement of its phonon–dispersion curve by Ohba et al [28] indeed revealed a fairly strong softening of $1/3 < 110 > \langle 1\bar{1}0 \rangle$ phonon mode, which is directly related to the martensite structure. This result is similar to that for another weak MT: B2–R transformation of Ti–Ni–Fe (transformation strain $\sim 1\%$) [56]. On the other hand, 'harder' MTs in Cu-based alloys (e.g. Cu–Zn–Al [79], Cu–Al–Ni [80,81], Cu–Al–Be [82]) seem to exhibit only a relatively weak softening in $<110> \langle 1\bar{1}0 \rangle$ phonon branch with only a very shallow dip around $1/3 < 110 > \langle 1\bar{1}0 \rangle$ and with a small temperature dependence, and the relation between the softening phonon and martensite structure is not evident. It is interesting to note that in these alloys many martensites differing from the thermally induced one can be formed under stress [83]. This seems to suggest that the lattice softening of the parent phase should contain the information about several possible martensite candidates, not just the one that forms thermally. If this is true, it becomes no longer surprising why the phonon dip does not

always predict the correct martensite structure, because it may only tell the possible candidates, and the actual martensite formed is determined not only by the phonon softening (i.e. harmonic energy) but also by anharmonic energy which cannot be directly ascertained from the dispersion relation. Nagasawa et al. [84,85] found that a specific combination of two interplanar force constants can reproduce the main features (the shallow 1/3 dip) of the TA_2 phonon dispersion of Cu-based alloys and thus they concluded that the $1/3 < 110 > \langle 1\bar{1}0 \rangle$ phonon dip is not a martensite precursor. However, they admit that this conclusion is not applicable to other alloys because it is of little doubt that such a dip in other alloys (e.g. Au–Cd and Ti–Ni) is a true precursor.

Another frequently reported precursor phenomenon is the appearance of diffuse scattering in diffraction pattern [86–88] and the corresponding real space image: tweed [87,88]. First we would like to point out that diffuse scattering or tweed does not generally exist in all martensitic alloys. Diffuse scattering or tweed has not been reported in some alloys undergoing strongly 1st order MT, such as alkali metals and some ferrous alloys (here we exclude those tweeds irrelevant to MT, e.g. due to the decomposition of the parent phase). The superlattice diffuse scattering is related to a 'central-mode' [67], indicating the existence of static embryo above transformation temperature. Such central-mode has been found in 2nd order transformations and in many weakly or moderately 1st order transformations, but seems to be absent at least in some of the strongly 1st order MT such as in alkali metals and probably in some ferrous alloys. It has also been reported that the static precursor (central-mode) is absent in pure systems without point defects [89]. This seems to suggest that point defects may play a role in producing the diffuse scattering or tweed. Until now no general explanation of the existence or the absence of precursory diffuse scattering/tweed is available, and more experimental and theoretical work should be done.

6.4. Origin of the martensitic transformations

It is of interest to discuss the origin of MT, i.e. what is the driving force for such a transformation? Although it is still a subject of dispute, it seems that on the level of lattice dynamics almost all different 1st order MTs can find a common origin: 1st order MT is driven dominantly by phonon entropy difference between parent phase and martensite [90,91]. The parent phase has higher vibrational entropy because its low-lying or soft phonon branch contributes significantly to the entropy of the system. On the contrary, stiffer martensite has lower vibrational entropy due to its higher phonon energy. As a result, a transformation from a high entropy state (parent phase) to a low

entropy state (martensite) will definitely occur at some temperature (usually not very high), according to the basic principle of thermodynamics that a low entropy state is favored at low temperatures and a high entropy state is favored at high temperatures. Planes and coworkers [92,93] have studied MT in Cu-based shape memory alloys using elastic constant measurements and calorimetry measurements. Their results also suggest a dominant phonon contribution to entropy.

Nevertheless, if we want to know why phonons soften in the parent phase, it appears that the possible answer may vary from alloy to alloy. For example, it has been suspected that many MTs can be caused by certain electron effect, which can induce a phonon anomaly through electron–phonon coupling [94]. However, MT in ferrous alloys or other magnetic alloys certainly has a different origin: it is largely due to the magnetic contribution. For example, there has been some clear evidence indicating the softening in elastic constants in Fe–Ni and Fe–Pt alloy can be ascribed to the magnetoelastic coupling between magnetization and phonons [95,96]. MT in Ni_2MnGa also appears to have a magnetic origin [97]. Therefore, it seems that the microscopic origin of MTs may be diverse and depends on specific alloy systems, although they can find a general and unified phenomenological understanding in terms of lattice dynamics and thermodynamics.

Ahlers [98] used a different phenomenological approach to study phase stability for β-phase alloys. He applied conventional Bragg–Williams method to calculate enthalpy of different phases, while using an empirical relation to evaluate vibrational entropy change during MT. By choosing suitable fitting parameters, this treatment seems to give a reasonable fit to experimental data. However, this model seems difficult to apply to other alloys (e.g. Ti–Ni) because the empirical relations may no longer be valid in that case.

7. Martensite aging and rubber-like behavior of martensite

The origin of martensite aging and the associated rubber-like behavior has been a long-standing puzzle for alloys undergoing MT, and the martensite aging effect is detrimental to the reliability of devices using shape memory alloys because it causes an increase in reverse transformation temperature (switching temperature). Therefore, understanding the origin of martensite aging effect is of both fundamental and practical importance. In view of the recent progress [99], we feel that now we can give a general answer to the problem, and as a consequence we can propose a guideline to prevent the aging effect. Due to page limit, we can give only a concise introduction of recent progress. The interested reader may refer to recent reviews [100,101] for details.
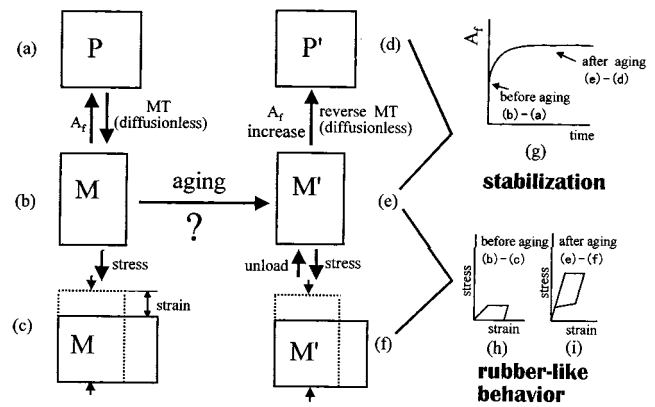

Fig. 11. Relationship among martensitic transformation, martensite aging, martensite stabilization and rubber-like behavior. P and M refer to the parent phase and the martensite, respectively [99].

Martensite aging phenomena include two closely related time-dependent effects after MT, as shown in Fig. 11 [102]. One is the so-called 'martensite stabilization', by which martensite becomes more stable with aging, such that the reverse transformation finish temperature (A_f) increases with aging time (Fig. 11(g)). Another is the 'rubber-like behavior (RLB)', in which that martensite exhibits recoverable or pseudo-elastic deformation behavior after being aged for some time (Fig. 11 (i)). The most puzzling problem with the RLB is why there should exist a restoring force, since martensite deformation involves only twinning and no phase transformation is involved, unlike that of superelasticity of the parent phase (i.e. due to stress-induced martensitic transformation). The central question concerning the martensite aging effect is: 'what is happening during martensite aging which gives rise to stabilization and the RLB?'

Many of previous studies on Cu-based alloys concluded that some structure change in martensite during aging is responsible for the aging effect. However, martensites of these alloys are unstable (i.e. non-equilibrium phases), and thus they have an inborn tendency to decompose simultaneously during aging. Therefore, the observed structure change may be just due to the inadvertent decomposition (maybe partially), while aging itself may be independent of the decomposition. Recent extensive experiments on stable or equilibrium martensites Au–Cd [103–105] and Au–Cu–Zn [106] (without the decomposition problem) proved that aging develops even without any detectable change in average martensite structure, as shown in Fig. 12. This seemingly perplexing result is in fact very natural: the average structure of an equilibrium or stable phase is not expected to depend on time (aging). Then the remaining puzzle is how a significant change in mechanical properties and transformation behavior can be realized without lending to average structure changes.

A correct mechanism must explain *all* of the general features of martensite aging listed below:

1. Aging is a time-dependent process.
2. Aging is not dependent on a change in the average structure of martensite [99,103–106].
3. Aging appears even in single-variant martensite where no variant (twin) boundary exists [107,108,105].
4. Aging effect is sensitive to point defects [109,105].
5. Aging phenomena occur both in ordered and disordered martensites.
6. Aging phenomena do not rely on the specific structure of martensite (i.e. aging can occur in any martensite).

None of the previous models completely explained all of the above features. The boundary pinning model [110] failed to explain (3), and long-range ordering (LRO) models (i.e. change of LRO during aging) by Abu Arab and Ahlers [111] and by Tadaki et al. [112] failed to explain (2), (5) and (6). Recent models by Marukawa and Tsuchiya [113], Suzuki et al. [114] emphasize the role of short range ordering (SRO), which was first proposed by Ahlers et al. [115]. Although this is a step toward the correct goal, these models still fail to explain all of the above features. For example, Marukawa's model, together with Ahlers' model, cannot explain (2) (5) and (6), while Suzuki's model cannot explain (2) and requires an excessive amount of point defects ($\approx 10\%$). The problem with these SRO models is that they define SRO in such a way that it is closely connected to LRO (i.e. average structure). As a result, the change in SRO will simultaneously cause a corresponding change in LRO, and thus these SRO can be viewed as different versions of LRO models. However, they contradict the experimental fact (2).
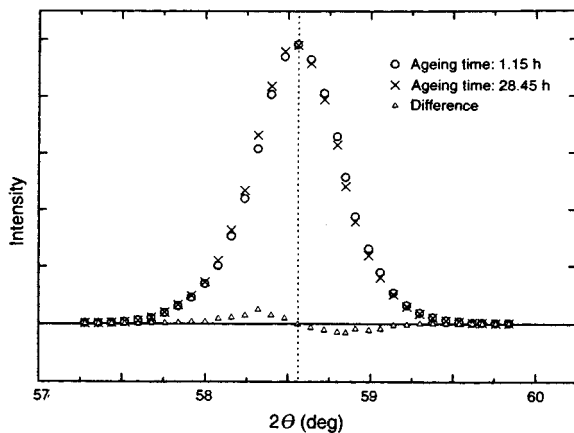

Fig. 12. X-ray profiles of (242) Bragg reflection of Au–47.5at%Cd martensite after aging for short (1.15 h) and long (28.45 h) time, respectively (After Ohba, Otsuka, Sasaki [103]). No change in peak position and intensity is found, except for a slight change in the symmetry of the peak. Such a change can find an explanation in the SC–SRO mechanism [99].
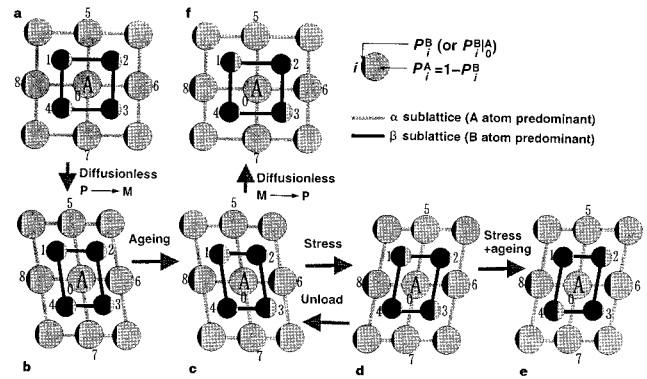

Fig. 13. Symmetry-conforming short-range order mechanism of martensite aging phenomena [99]. The illustrations show the statistical atomic configuration (conditional probabilities around an A atom) of an *imperfectly ordered* A–B alloy in, (a) equilibrium parent phase; (b) martensite immediately after transformed from (a); (c) equilibrium martensite; (d) stress-induced martensite variant (twin) immediately formed from (c); (e) equilibrium state of the stress-induced variant; and (f) parent immediately transformed from (c), respectively. P: the parent phase, and M: martensite. P_i^B (or P_i^A) is the conditional probability of B atom (or A atom) occupying i-site ($i = 1, 2, 3, ..., 8$) if an A atom is at 0-site. The relative values of P_i^B and P_i^A are indicated by the black and gray areas, respectively.

Very recently Ren and Otsuka [99] proposed a general model to explain the origin of martensite aging. They suggested that the aging phenomena stem from a general tendency that the symmetry of short-range order configurations of point defects tries to conform or follow the symmetry of the crystal. This is named symmetry-conforming short-range order principle (or SC-SRO principle) of point defects, and is applicable to any crystal containing point defects.

The SC-SRO principle gives a general and simple explanation to the aging phenomena. Fig. 13.a shows a two-dimensional A–B binary *imperfectly ordered* parent phase with 4-fold symmetry. (The same idea is applicable to any 3-D martensite). Because of the 4-fold symmetry of the structure, the probability of finding a B atom about the A atom (or B atom) must possess the same 4-fold symmetry according to SC-SRO principle, i.e. $P_1^B = P_2^B = P_3^B = P_4^B$, and $P_5^B = P_6^B = P_7^B = P_8^B$ etc., where P_i^B ($i = 1, 2, 3, ...$) are conditional probabilities, as defined in Fig. 13.

When the parent phase shown in Fig. 13a transforms diffusionlessly into martensite, all the probabilities must remain unchanged despite the symmetry change, as shown in Fig. 13b. That is, $P_1^B = P_2^B = P_3^B = P_4^B$, and $P_5^B = P_6^B = P_7^B = P_8^B$ etc. However, this high-symmetry configuration is no longer a stable configuration for the lower symmetry martensite structure according to the SC-SRO principle. Then during aging, such a configuration gradually changes into a stable one that conforms to martensite symmetry, as shown in Fig. 13c. Because the equilibrium martensite structure should be maintained (for stable martensite), this process pro-

ceeds by atomic rearrangement or relaxation within the same sublattice. This is the only way that a martensite can lower its free energy without altering the average structure (equilibrium phase).

When the stabilized (or aged) martensite (Fig. 13c) is deformed, it changes into another variant (i.e. twin) as a result of the accommodation of the strain. Because this twinning process is also diffusionless, the atomic occupation probabilities shown in Fig. 13c is inherited to the new variant, as shown in Fig. 13d. Such a configuration, however, is not the stable one for the new variant, which is shown in Fig. 13e. Therefore, a driving force that tries to restore the original variant (Fig. 13c) engenders. When the external stress is released immediately after the loading, this restoring force reverts the new variant (Fig. 13d) to the original one (Fig. 13c) by de-twinning. This is the origin of the rubber-like behavior.

When the stabilized martensite (Fig. 13c) is heated up and transforms back (diffusionlessly) into the parent, the stable SRO configuration for the martensite is inherited into the parent (Fig. 13f). From the above-mentioned symmetry-conforming principle of SRO, it is obvious that Fig. 13f is not a stable configuration for the parent. From a thermodynamic point of view, this corresponds to an increased reverse transformation temperature. This is the origin of martensite stabilization.

The SC-SRO model can be easily extended into disordered alloys by considering the existence of only one sublattice. In this case, the present model reduces to Christian's model [116], which was later elaborated by Otsuka and Wayman [117]. This model explained the rubber-like elasticity in disordered alloys such as In–Tl.

The largest advantage of the SC-SRO model compared with previous models is its generality. It not only explains why aging does not need a change of average structure of martensite, but also unified the origin of aging effect for both ordered and disordered martensites. It is also applicable to any martensite because it is only related with crystal symmetry, not the structure details of martensite or parent phase. The generality of the model lies in that it makes use of only two general features of martensitic transformation and aging: diffusionless symmetry-change upon martensitic transformation (without relying on specific martensite structure),

and (short-range) diffusion of point defects during aging. In line with this reasoning, it can be deduced that the existence of point defects and possibility of diffusion in martensite are two necessary conditions for aging phenomena. The existence of point defects is generally satisfied by alloys, but the possibility of diffusion in martensite depends on the reduced martensitic transformation temperature M_s/T_m, where M_s and T_m are martensitic transformation start temperature and melting point of alloy. The higher this reduced temperature is, the faster diffusion in martensite becomes. If this value is too low, aging phenomena are too slow to be observed; if this value is too high, aging is so fast that aging actually completes immediately after the martensitic transformation, thus the time-dependence of aging may not be observed. As shown in Table 1 [100], Ti–Ni alloy belongs to the former case, and In–Tl belongs to the latter. Other shape memory alloys are in-between. Thus, this gives an answer to an important problem as to why some alloys show a strong aging effect while others show little. From Table 1, we can see that a low M_s/T_m ratio (< 0.2) is necessary in order to avoid the aging effect. It is an important guideline to design SMAs without the unwanted aging effect.

From the above we can see that point defects in shape memory alloys play a central role in determining martensite aging effects. However, many investigations neglected an important fact: most shape memory alloys are in fact ordered alloys or intermetallics, and the defect structure and concentration is quite different from that in pure metals or disordered alloys [118]. Therefore, information on the defect structures and concentrations is important for a deep understanding of the effect of defects on aging. Otsuka et al. [119] measured the composition dependence of the defect concentration of Au–Cd alloys and found a strong correlation between RLB and defect concentration. Their result supports the SC-SRO mechanism of martensite aging.

8. Martensite and deformation

Martensite and deformation have a close relation in various respects, since stress affects the free energies of parent and martensite, and MT itself and twinning in

Table 1
Relationship between the reduced martensitic transformation temperature M_s/T_m and the rate of martensite aging (RLB) at room temperature [100]

Alloy	Ti–Ni	Cu–Al–Ni	Cu–Zn–Al	Au–Cd	In–Tl
M_s/T_m	≈ 0.19	≈ 0.23	≈ 0.27	≈ 0.34	0.50–0.79
Aging time for RLB at R.T.	$\approx \infty$ (i.e. no aging effect)	≈ 10 months	≈ 5 h	≈ 0.5 h	< 1 s

martensite act as deformation modes under an applied stress. Typical cases are the shape memory effect and superelasticity. The two-way memory effect and 'training' are the results of the interaction of residual strains and MT. The effect of deformation on the M_s temperature has been known for a long time. In this section, we will pick up two rather recent topics in this respect.

When we use SMA for actuator applications, we need a MT with a small temperature hysteresis. However, when we use SMA for coupling applications, a transformation with a larger temperature hysteresis is desirable in order to store a deformed coupling before joining at ambient temperature. In the course of the study of SMA for couplings, Melton et al. [120–122] found that the pre-deformation of martensites in Ti–Ni–Nb alloys remarkably increases the A_s temperature, A_s increasing with increasing pre-deformation, and this A_s increase annihilates, once the specimen is subjected to the reverse transformation by heating. This peculiar phenomenon was analyzed by Piao et al. [123] as follows, and it was shown that the phenomenon is characteristic not only of Ti–Ni–Nb but also of other thermoelastic alloys.

It is well-known that elastic energy is stored during thermoelastic MT. More specifically, Olson and Cohen [124] formulated the following equation for a thermodynamic equilibrium between a martensite plate and the surrounding parent phase:

$$\Delta g_{ch} + 2\Delta g_{el} = 0,$$

where $\Delta g_{ch} = g_M - g_P$ is the chemical free energy between parent and martensite, and Δg_{el} is the elastic strain energy stored around the martensite plate. The above equation means that half of the chemical free energy change is stored as the elastic energy in the specimen during the forward transformation. This elastic energy is expected to resist the forward transformation, and to assist the reverse transformation. That is, in the actual materials the A_s temperature is lowered from that of the material itself because of the presence of the elastic energy. Thus, if we release the elastic energy by some means, we can expect to increase the A_f temperature toward that of the material itself. This is the essence of Piao et al.'s idea. To prove the idea, they carried out a simple experiment using a Cu–Al–Ni single crystal. Fig. 14 shows resistance vs. temperature curve in cooling–heating cycles. (a) represents such a cycle without deformation. In (b) the specimen was cooled below M_f (martensite finish temperature) first, and was then tensile tested until the end of the 1st stage of the stress–strain curve, and was then heated until the reverse transformation occurred. Here we can clearly see that A_s increased substantially by the pre-deformation in martensite. (c) represents the resistance vs. temperature curve in the next cycle after the experiment in (b). We notice that A_s returned to the original value in
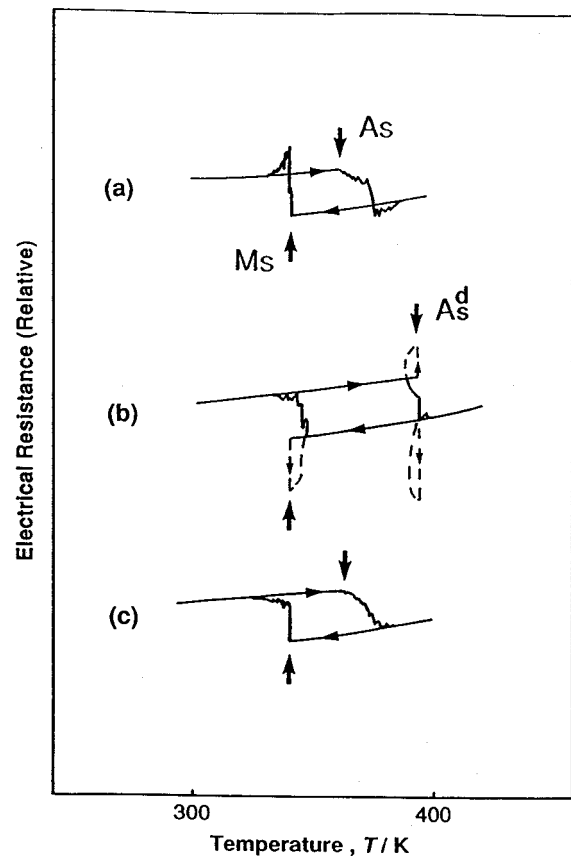

Fig. 14. Electrical resistance vs. temperature curves of a Cu–13.8Al–4.0Ni single crystal. (a) before tensile test, (b) first cycle after tensile test, (c) after the cycle in (b) [123]. See text for details.

(a). The result of this experiment is easily explained as follows. After the specimen was cooled below M_f, it is in multi-variant state with many twins. By the application of stress, these twins were eliminated by de-twinning. Thus, strains were released from the surface of the specimen, leading to the increase of A_s. In the third cycle of (c), the specimen became a multi-variant state again. Thus, A_s returned to the initial value in (a). Thus, the behavior was explained completely by the above idea. Similar experiments were carried out for polycrystalline Ti–Ni alloys. In the case of polycrystals strains can not be released from the surface of specimens, since the constraints of grain boundaries are present. In this case, strains are relaxed by the introduction of slip instead, but the behavior can be explained in a similar manner. See the original paper for more details. Thus, we have shown that the elastic energy stored in thermoelastic transformation is responsible for the A_s increase by pre-deformation in martensite.

The second topic concerns the shape memory behavior and plastic deformation. The assessments of SME performance are usually done by taking strain vs. temperature curve under constant load as shown in Fig. 15, which was taken for a solution-treated Ti–42Ni–8Cu

alloy. In a cooling-heating cycle, the loop is closed if no plastic strain is introduced in the cycle. However, if permanent strain is introduced, a gap is made between the initial line and the final line, as typically shown in the upper top curve. The central problem here is when the plastic strain is introduced. Probably people usually think that the plastic strain is introduced in the forward transformation, since the strain produced in the forward transformation is larger than that in the reverse transformation, as noted first by Liu and McCormic [125]. However, Tan [126] showed by a simple experiment that this is not correct.
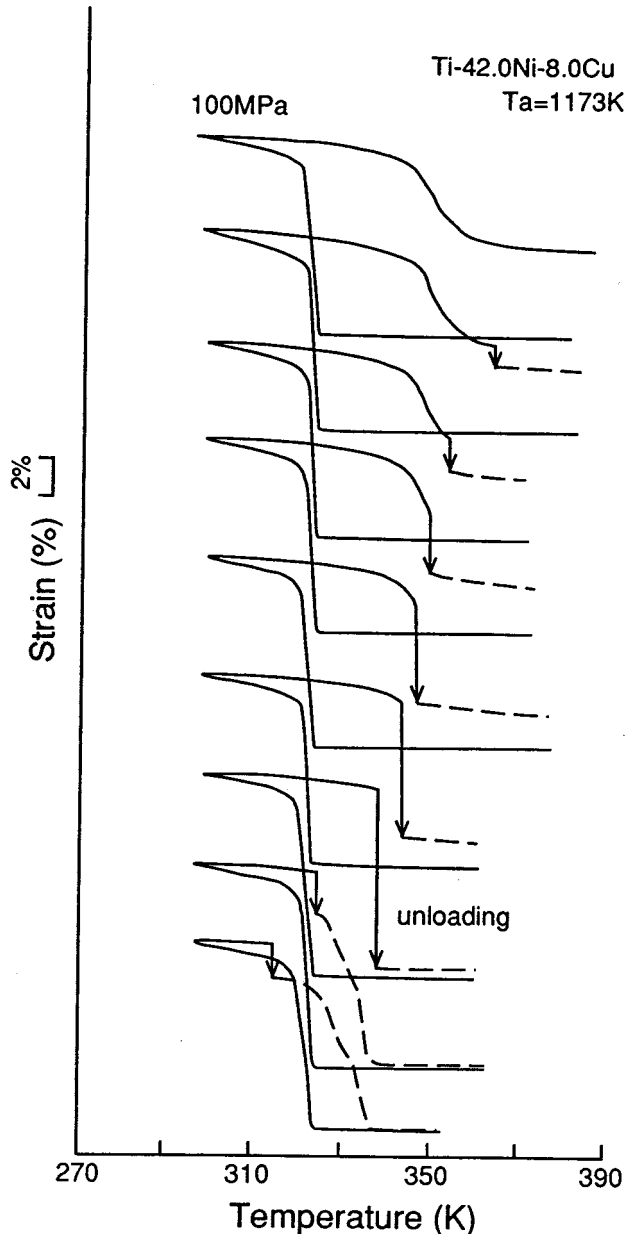

Fig. 15. Strain vs. temperature curves of Ti–42.0Ni–8.0Cu alloy under constant stress of 100 MPa upon cooling and subsequent unloading at various temperatures in the absence of stress (dotted lines) [126]. See text for details.

Referring to Fig. 15, Tan carried out such an experiment that in cooling–heating cycle, the load was eliminated at various temperatures during heating. Thus, in Fig. 15 the vertical arrows indicate strain relaxation during the load elimination, and dotted lines strain recovery by the virtue of SME in the absence of load. Thus, the lowest curve indicates that if the load is eliminated at temperatures below A_s, complete SME is obtained. This means that the plastic strains are not introduced in the forward transformation but in the reverse transformation. This may be explained in the following way. Since the martensites are formed under load upon cooling, the load assists the forward transformation, and thus resists the reverse transformation of particular variants. Thus, the A_f temperature under load is increased compared to that without load, as shown in the figure. This resistive force is equivalent to the excess load for the specimen, which permits strain by slip in the direction of the load. From the above experiment it is clear that the permanent strain is introduced in the reverse transformation.

Acknowledgements

References

[1] T.B. Massalski, H. Okamoto, P.R. Subramanian, L. Kacprzac (Eds.), Binary Alloy Phase Diagrams, vol. 3, 2nd edn, ASM International, OH, 1990, p. 2875.
[2] P. Duez, J.L. Taylor, Trans. AIME 188 (1950) 1173.
[3] H. Margolin, E. Ence, J.P. Nielsen, Trans. AIME, J. Metals February (1953) 243.
[4] D.M. Poole, W. Hume-Rothery, J. Inst. Metals 83 (1954) 473.
[5] R.J. Wasilewski, S.R. Butler, J.E. Hanlon, D. Worden, Met. Trans. 2 (1971) 229.
[6] D. Koskimaki, M.J. Marcinkowski, A.S. Sastri, Trans. AIME 245 (1969) 1883.
[7] M. Nishida, C.M. Wayman, T. Honma, Met. Trans. 17A (1986) 1505.
[8] T. Honma, T. Matsumoto, Y. Shugo, M. Nishida, Res. Rep. Nucl. Sci. Lab. Tohoku Univ. 12 (2) (1979) 183.
[9] M. Nishida, C.M. Wayman, T. Honma, Scripta Met. 19 (1985) 983.
[10] T. Tadaki, Y. Nakata, K. Shimizu, K. Otsuka, Trans. JIM 27 (1986) 731.

[11] T. Saburi, S. Nenno, T. Fukuda, Less Com. Metals 125 (1986) 157.

[12] S. Miyazaki, Y. Ohmi, K. Otsuka, Y. Suzuki, J. Phys. (France) 43 (1982) C4–255.

[13] T. Saburi, T. Tatsumi, S. Nenno, J. Phys (France) 43 (1982) C4–261.

[14] S. Miyazaki, K. Otsuka, Met. Trans. 17A (1986) 53.

[15] M. Nishida, T. Honma, Scripta Met. 18 (1984) 1293.

[16] S. Miyazaki, Mater. Sci. Eng. A273–275 (1999) 660–665.

[17] H. Okamoto, J. Phase Equilibria 14 (2) (1993) 257.

[18] K. Enami, S. Nenno, Trans. JIM 19 (1978) 571.

[19] I.M. Robertson, C.M. Wayman, Metallography 17 (1984) 43.

[20] P.S. Khadkikar, K. Vedula, J. Mater. Res. 2 (1987) 163.

[21] J.H. Yang, C.M. Wayman, Mater. Sci. Eng. A160 (1993) 241.

[22] J.H. Yang, C.M. Wayman, Intermetallics 2 (1994) 111, 121.

[23] P.S. Khadkikar, I.E. Locci, K. Vedula, G.M. Michal, Met. Trans. 24A (1993) 83.

[24] Y. Murakami, K. Otsuka, Mater. Sci. Eng. A189 (1994) 191.

[25] A. Ölander, Z. Krist. 83A (1932) 145.

[26] T. Ohba, Y. Emura, S. Miyazaki, K. Otsuka, Mater. Trans. JIM 31 (1990) 12.

[27] T. Ohba, Y. Emura, K. Otsuka, Mater. Trans. JIM 33 (1992) 29.

[28] T. Ohba, S.M. Shapiro, S. Aoki, K. Otsuka, Jpn. J. Appl. Phys. 33 (1994) L1631.

[29] Y. Kudoh, M. Tokonami, S. Miyazaki, K. Otsuka, Acta Met. 33 (1985) 638.

[30] G.R. Purdy, J.G. Parr, Trans. AIME 221 (1961) 631.

[31] K. Otsuka, T. Sawamura, K. Shimizu, Phys. Stat. Sol. 5A (1971) 457.

[32] R.F. Hehemann, G.D. Sandrock, Scripta Met. 5 (1971) 801.

[33] G.M. Michal, R. Sinclair, Acta Crystallogr. B37 (1981) 1803.

[34] W. Bührer, R. Gotthardt, A. Kulik, O. Mercier, F. Staub, J. Phys. F: Met. Phys. 13 (1983) L77.

[35] D.P. Dautovich, G.R. Purdy, Can. Metall. Q. 4 (1965) 129.

[36] S. Vatanayon, R.F. Hehemann, in: J. Perkins (Ed.), Shape Memory Effects in Alloys, Plenum, New York, 1975, p. 115.

[37] E. Goo, R. Sinclair, Acta Met. 33 (1985) 1717.

[38] T. Hara, T. Ohba, E. Okunishi, K. Otsuka, Mater. Trans. JIM 38 (1997) 11.

[39] K. Otsuka, Materials Science Forum 56–58 (1990) 393.

[40] T. Tadaki, Y. Katano, K. Shimizu, Acta Met. 26 (1978) 883.

[41] H.M. Ledbetter, C.M. Wayman, Acta Met. 20 (1972) 19.

[42] S. Aoki, K. Morii, Y. Murakami, K. Otsuka, Proceedings of Solid–Solid Phase Transformations, Pittsburgh, PA, 1994, p. 779.

[43] K. Otsuka, T. Ohba, Y. Murakami, in: K. Inoue, et al. (Eds.), Displacive Phase Transformations and Their Applications in Materials Engineering, TMS, 1998, p. 167.

[44] T. Fukuda, T. Saburi, K. Doi, S. Nenno, Mater. Trans. JIM 33 (1992) 271.

[45] T. Saburi, S. Nenno, Proceedings of the International Conference on Solid–Solid Phase Transformations, AIME, New York, 1982, p. 1455.

[46] J.W. Christian, A.G. Crocker, in: F.R.N. Nabarro (Ed.), Dislocation Theory: A Collective Treatise, vol. 3, North-Holland, Amsterdam, 1980.

[47] K.M. Knowles, Phil. Mag. 45A (1982) 357.

[48] T. Hara, T. Ohba, K. Otsuka, Y. Bando, S. Nenno, Proceedings of ICOMAT-92, Monterey, 1992, p. 257.

[49] T. Hara, T. Ohba, K. Otsuka, Proceedings of PRICM-3, Hawaii, TMS, 1998, p. 1199.

[50] M. Nishida, K. Yamauchi, I. Itai, H. Ohgi, A. Chiba, Acta Met. Mater. 43 (1995) 1229.

[51] M. Hwang, M. Meichle, M.B. Salamon, C.M. Wayman, Phil. Mag. 47A (1983) 9–31.

[52] T. Tamiya, D. Shindo, Y. Murakami, Y. Bando, K. Otsuka, Mater. Trans. JIM 39 (1998) 714.

[53] M.B. Salamon, M.E. Meichle, C.M. Wayman, Phys. Rev. B31 (1985) 7306.

[54] S.M. Shapiro, Y. Noda, Y. Fujii, Y. Yamada, Phys. Rev. B30 (1984) 4314.

[55] M.B. Salamon, M.E. Meichle, C.M. Wayman, C.M. Hwang, S.M. Shapiro, in: J.M. Cowley, et al. (Eds.), Modulated Structures (Kailua Kona, Hawaii), Proceedings of the International Conference on Modulated Structures, AIP, New York, 1979, p. 223.

[56] S.K. Satija, S.M. Shapiro, M.B. Salamon, C.M. Wayman, Phys. Rev. B29 (1984) 6031.

[57] H.C. Ling, R. Kaplov, Met. Trans. 11A (1980) 77.

[58] Y. Yamada, Proceedings of ICOMAT-86, JIM, Sendai, 1986, p. 89.

[59] T. Saburi, Proceedings of ICOMAT-92, Monterey Institute for Advanced Studies, Monterey, 1992, p. 857.

[60] Y. Murakami, D. Shindo, K. Otsuka, Annual Fall Meeting of JIM, Matsuyama, September, 1998.

[61] W. Cai, Y. Murakami, K. Otsuka, Mater. Sci. Eng. A273–275 (1999) 186–189.

[62] Y. Noda, M. Takimoto, T. Nakagawa, Y. Yamada, Met. Trans. 19A (1988) 265.

[63] T. Ohba, K. Otsuka, MRS Proc. 459 (1997) 295.

[64] L.R. Testardi, T.B. Bateman, W.A. Reed, V.G. Chirba, Phys. Rev. Lett. 15 (1965) 250.

[65] W. Rehwald, Phys. Lett. 27A (1968) 287.

[66] D.J. Gunton, G.A. Saunders, Solid State Commun. 14 (1974) 865.

[67] S.M. Shapiro, B.X. Yang, G. Shirane, Y. Noda, L.E. Tanner, Phys. Rev. Lett. 62 (1989) 1298.

[68] G. Ernst, C. Artner, O. Blaschko, G. Krexner, Phys. Rev. B33 (1986) 6465.

[69] O. Blaschko, G. Krexner, Phys. Rev. B30 (1984) 1667.

[70] G. Shirane, Rev. Mod. Phys. 46 (1974) 437.

[71] J.A. Krumhansl, R.J. Gooding, Phys. Rev. 39 (1989) 3047.

[72] C. Zener, Phys. Rev. 71 (1947) 846.

[73] X. Ren, K. Otsuka, Scripta Mater. 38 (1998) 1669.

[74] O. Mercier, K.N. Melton, G. Gremaud, J. Hagi, J. App. Phys. 51 (1980) 1833.

[75] X. Ren, K. Taniwaki, K. Otsuka, T. Suzuki, K. Tanaka, Yu.I. Chumlyakov, T. Ueki, Philo. Mag. 79A (1999) 31.

[76] X. Ren, N. Miura, K. Taniwaki, K. Otsuka, T. Suzuki, K. Tanaka, Yu.I. Chumlyakov, M. Asai, Mater. Sci. Eng. A273–275 (1999) 190–194.

[77] T.N. Nam, T. Saburi, K. Shimuzu, Mater. Trans. JIM 31 (1990) 959.

[78] N. Nakanishi, Prog. Mater. Sci. 24 (1980) 143.

[79] G. Guenin, S. Hantecler, R. Pynn, P.F. Gobin, L. Delaey, Scripta Metall. 13 (1979) 429.

[80] S. Hoshino, G. Shirane, M. Suezawa, T. Kajitani, Jpn. J. Appl. Phys. 14 (1975) 1233.

[81] Y. Morii, Iizumi, J. Phys. Soc. Jpn. 54 (1985) 2940.

[82] Ll. Manõsa, J. Zarestky, T. Lograsso, D.W. Delaney, C. Stassis, Phys. Rev. B48 (1993) 15708.

[83] K. Otsuka, H. Sakamoto, K. Shimizu, Acta Metall. 27 (1979) 585.

[84] A. Nagasawa, A. Yoshida, T. Makita, Trans. JIM 30 (1989) 639.

[85] A. Nagasawa, Y. Morii, Mater. Trans. JIM 34 (1993) 855.

[86] K. Otsuka, C.M. Wayman, H. Kubo, Metall. Trans. 9A (1978) 1075.

[87] L.E. Tanner, A.R. Pelton, R. Gronsky, J. Phys. (Paris) Colloq. 43 (1982) C4–169.

[88] D. Schryvers, L.E. Tanner, Ultramicroscopy 32 (1990) 241.

[89] W. Petry, T. Flottmann, A. Heiming, J. Trampenau, M. Alba, G. Vogl, Phy. Rev. Lett. 61 (1988) 722.

[90] S. Alexander, J.P. McTague, Phys. Rev. Lett. 41 (1978) 702.

[91] R.J. Gooding, J.A. Krumhansl, Phys. Rev. B38 (1988) 1695.

[92] A. Planes, Ll. Manõsa, D. Rios-Jara, J. Ortin, Phys. Rev. B45 (1992) 7633.

[93] Ll. Manõsa, A. Planes, J. Ortin, B. Martinez, Phys. Rev. B48 (1993) 3611.

[94] S.K. Sinha, in: G.K. Horton, A.A. Maradudin (Eds.), Dynamical Properties of Solids, North-Holland, New York, 1980, p. 1.

[95] G. Hausch, H. Warlimont, Acta Metall. 21 (1973) 401.

[96] G. Hausch, J. Phy. Soc. Jpn. 37 (1974) 819.

[97] A. Planes, E. Obrado, A. Gonzalez-Comas, Ll. Manõsa, Phys. Rev. Lett. 79 (1997) 3926.

[98] M. Ahlers, J. Phys. IV 5 (1995) C8–71.

[99] X. Ren, K. Otsuka, Nature 389 (1997) 579.

[100] K. Otsuka, X. Ren, Proceedings of the 3rd Pacific Rim International Conference on Advanced Materials and Processing, Honolulu, HI, USA, July 12–16, 1998, TMS, 1998.

[101] X. Ren, K. Otsuka, Phase Transitions (1999) in press.

[102] X. Ren, K. Otsuka, Mater. Jpn. 37 (1998) 498 (in Japanese).

[103] T. Ohba, K. Otsuka, S. Sasaki, Mater. Sci. Forum 56–58 (1990) 317.

[104] Y. Murakami, Y. Nakajima, K. Otsuka, T. Ohba, J. Phys. III C8-5 (1995) 1071.

[105] Y. Murakami, Y. Nakajima, K. Otsuka, T. Ohba, R. Matsuo, K. Ohshima, Mater. Sci. Eng. A237 (1997) 87.

[106] T. Ohba, T. Finlayson, K. Otsuka, J. Phys. III C8-5 (1995) 1083.

[107] R. Rapacioli, M. Chandrasekaran, M. Ahlers, L. Delaey, in: J. Perkins (Ed.), Shape Memory Effects in Alloys, Plenum Press, New York, 1975, p. 365.

[108] G. Barcelo, R. Rapacioli, M. Ahlers, Scripta Metall. 12 (1978) 1069.

[109] Y. Nakajima, S. Aoki, K. Otsuka, T. Ohba, Mater. Lett. 21 (1994) 271.

[110] N. Nakanishi, T. Mori, S. Miura, Y. Murakami, S. Kachi, Philos. Mag. 28 (1973) 277.

[111] A. Abu Arab, M. Ahlers, Acta Metall. 36 (1988) 2627.

[112] K. Marukawa, K. Tsuchiya, Scripta Metall. 32 (1995) 77.

[113] T. Tadaki, H. Okazaki, Y. Nakata, K. Shimizu, Mater. Trans. JIM 31 (1990) 941.

[114] T. Suzuki, T. Tonokawa, T. Ohba, J. Phys. III C8-5 (1995) 1065.

[115] M. Ahlers, G. Barcelo, R. Rapacioli, Scripta Metall. 12 (1978) 1075.

[116] J.W. Christian, The Theory of Transformations in Metals and Alloys, Pergamon, Oxford, 1965, p. 789.

[117] K. Otsuka, C.M. Wayman, in: P. Feltham (Ed.), Review on the Deformation Behavior of Materials, vol. 2, Freund, Israel, 1977, p. 81.

[118] X. Ren, K. Otsuka, M. Kogachi, Scripta Mater. (1999) in press; Philo. Mag. (1999) in press.

[119] K. Otsuka, X. Ren, Y. Murakami, T. Kawano, T. Ishii, T. Ohba, Mater. Sci. Eng. A273–275 (1999) 559–564.

[120] K.N. Melton, J. Simpson, T.W. Duerig, Proceedings of ICOMAT-86, JIM, 1986, p. 1053.

[121] K.N. Melton, J.L. Proft, T.W. Duerig, Proceedings MRS. International Meeting on Advanced Materials Tokyo, 1989, p. 165.

[122] L.C. Zhao, T.W. Duerig, S. Justi, K.N. Melton, J.L. Proft, W. Yu, C.M. Wayman, Scripta Met. 24 (1990) 221.

[123] Min Piao, K. Otsuka, S. Miyazaki, H. Horikawa, Mater. Trans. JIM 34 (1993) 919.

[124] G.B. Olson, M. Cohen, Scripta Met. 9 (1975) 1247.

[125] Y. Liu, P.G. McCormic, ISIJ Int. 29 (1989) 417.

[126] S. Tan, Ph.D. Thesis, University of Tsukuba, 1998, p. 102.